Fabrication of Free-Standing, Electrochemically Active, and Biocompatible Graphene Oxide–Polyaniline and Graphene–Polyaniline Hybrid Papers

Xingbin Yan,*,†,‡ Jiangtao Chen,† Jie Yang,† Qunji Xue,† and Philippe Miele‡

State Key Laboratory of Solid Lubrication, Lanzhou Institute of Chemical Physics, Chinese Academy of Sciences, 18 Tianshui Mid. Road, Lanzhou 730000, China, and Laboratoire des Multimateriaux et Interfaces (UMR CNRS 5615), Université Lyon 1, Université de Lyon, 43 boulevard du 11 Novembre 1918, 69622 Villeurbanne Cedex, France

ABSTRACT In this work, we report a low-cost technique via simple rapid-mixture polymerization of aniline using graphene oxide (GO) and graphene papers as substrates, respectively, to fabricate free-standing, flexible GO–polyaniline (PANI) and graphene–PANI hybrid papers. The morphology and microstructure of the obtained papers were characterized by FESEM, FTIR, Raman, and XRD. As results, nanostructural PANI can be deposited on the surfaces of GO and graphene papers, forming thin, lightweight, and flexible paperlike hybrid papers. The hybrid papers display a remarkable combination of excellent electrochemical performances and biocompatibility, making the paperlike materials attractive for new kinds of applications in biosciences.

KEYWORDS: graphene oxide • graphene • polyaniline • supercapacitor • biocompatibility

INTRODUCTION

Graphene sheets, a new class of two-dimensional carbon nanostructure, because of their excellent electronic transport properties, extremely high mechanical stiffness, and exceptional thermal and electrical conductivity, have been predicted to hold great promise for many potential applications such as nanoelectronics, sensors, batteries, supercapacitors, hydrogen storage, and nanocomposites (1–5). To date, many approaches have been developed to prepare grapheme materials, mainly including micromechanical cleavage of highly oriented pyrolytic graphite (HOPG) (6), sublimation of silicon from silicon carbide (7), and some chemical methods (8, 9). As recently demonstrated by Ruoff and co-workers, graphene sheets can be prepared in large quantity through chemical conversion from graphite (10–12). They have also reported that, similar to carbon nanotubes, graphene oxide (GO) sheets can indeed be assembled into a paperlike material through flow-directed assembly by vacuum filtration of colloidal dispersion of GO sheets (13). More recently, liquid/air interface evaporation of GO hydrosol has also been employed to prepare macroscopic free-standing GO membranes (14). Also, Li and coworkers have recently reported that graphene paper can be prepared using the same strategy as has been used to make GO paper (15, 16). Such free-standing, paperlike GO and graphene materials have displayed excellent flexibility and mechanical stiffness combined with exceptional electrical conductivity (for graphene paper), and hence make them potentially suitable for flexible electrochemically active materials, such as fuel cells, electrical batteries, supercapacitors and biomedical devices (17). Nevertheless, the poor electrical conductivity of GO and the less-active surface of unitary graphene always prevent them from experiencing high electrochemical activity performance. Therefore, the incorporation of an electrically conductive and electrochemically active second phase in free-standing GO and graphene materials is very necessary to enhance their pristine electrochemical properties.

It is well-known that polyaniline (PANI) is one of the most promising conducting polymers. Because of the controllable conductivity, highly electrochemical activity, good biocompatibility, and low cost combined with the easiness of preparation, PANI materials have been widely studied as electrical, electrochemical, and biomaterials (18). Recently, extensive efforts have been made to prepare GO–PANI and graphene–PANI composite powders, which are expected to exhibit various functional properties (19–22). Especially, PANI has been considered to promote the electrochemical capacitance of GO and graphene materials (23–25).

In this paper, we present the preparation of free-standing GO–PANI and graphene–PANI hybrid papers via rapid-mixture polymerization of aniline on the surfaces of GO and graphene papers, respectively. This rapid-mixture polymerization is quite simple without the need of costly apparatus or the assistance of cooling or heating. More importantly, nanostructural PANI can be deposited on the surfaces of GO and graphene papers, forming thin, lightweight, and flexible hybrid papers. The obtained GO–PANI and graphene–PANI

* Correspondng author. E-mail: xbyan@licp.cas.cn.
Received for review March 31, 2010 and accepted July 30, 2010
† Chinese Academy of Sciences.
‡ Université de Lyon.
DOI: 10.1021/am100293r

hybrid papers display remarkably enhanced electrochemical properties compared with the parent GO and graphene papers, respectively, and exhibit excellent biocompatibility. The combination of flexibility, electrochemical activity, and biocompatibility makes such hybrid papers attractive for new kinds of applications in biosciences, such as electroactive substrates/scaffolds for tissue engineering, drug delivery, cell culture, and biosensors (26).

EXPERIMENTAL SECTION

2.1. Materials. Graphite powder (325 mesh) was purchased from Qingdao Huatai Tech. Co., Ltd. Aniline and ammonium peroxydisulfate (APS) were purchased from Sigma. Dimethyl sulfoxide (DMSO) and Dulbecco's modified Eagle's medium (DMEM) were purchased from Gibco. Trypsin-EDTA solution and 3-(4, 5-dimethyldiazol-2-yl)-2, 5-diphenyl tetrazolium bromide (MTT) were purchased from Sigma. Fetal bovine serum (FBS) was purchased from Hangzhou Sijiqing Biological Engineering Materials Co., Ltd. L-929 mouse fibroblast cells were supported by the School of Biological Sciences, University of Lanzhou, China. Other reagents were commercially available and of analytical reagent grade. Twice-distilled water with a resistance about 18 MΩ cm^{-1} was used throughout.

2.2. Preparation of GO-PANI and graphene-PANI hybrid papers. 2.2.1. ***Preparation of GO.*** GO was prepared from the natural graphite by following the methodology reported by Shi et al. (8, 27) In a typical synthesis, graphite powder (3 g, 325 mesh) was put into an 80 °C solution of concentrated H_2SO_4 (12 mL), $K_2S_2O_8$ (2.5 g), and P_2O_5 (2.5 g). The mixture was kept at 80 °C for 4.5 h using a hot plate. Successively, the mixture was cooled to room temperature and diluted with 0.5 L of H_2O and left overnight. The mixture was then filtered and washed with H_2O using a 0.45 μm Millipore filter to remove the residual acid. The product was dried under ambient condition. This preoxidized graphite was then subjected to oxidation by Hummers' method described as follows. Pretreated graphite powder was put into cold (0 °C) concentrated H_2SO_4 (120 mL). Then, $KMnO_4$ (15 g) was added gradually under stirring and the temperature of the mixture was kept to be below 20 °C by cooling. Successively, the mixture was stirred at 35 °C for 2 h, and then carefully diluted with 250 mL of H_2O. After that, the mixture was stirred for 2 h, and an additional 0.7 L of H_2O was then added. Shortly, 20 mL of 30% H_2O_2 was added to the mixture. The resulting brilliant-yellow mixture was filtered and washed with 10 wt % HCl aqueous solution (1 L) to remove metal ions followed by washed repeatedly with H_2O to remove the acid until the pH of the filtrate was neutral. The GO slurry was dried in a vacuum oven at 60 °C and purified by dialysis for 1 week.

2.2.2. ***Preparation of GO Aqueous Colloid and GO Paper.*** A fresh sample (200 mg) of GO solid was dispersed in 400 mL of H_2O with the aid of ultrasonication using a high-power (800W) ultrasonic pole at 0 °C for 60 min, followed by centrifugation at 3000 rpm min^{-1} for 15 min to remove a small quantity of precipitation, forming a black-brown GO aqueous colloid. This homogeneous dispersion was tested to be stable for several months. Twenty milliliters of the above colloid was diluted with 20 mL of H_2O and GO paper was prepared by filtration of the diluted dispersion through an Millipore filter (50 mm in diameter and 0.45 μm in pore size), followed by washing, air drying, and peeling off from the filter.

2.2.3. ***Preparation of Graphene Paper.*** In a typical reduction procedure from GO to graphene, 20 mL of GO colloid was mixed with 20 mL of H_2O, 17.5 μL of hydrazine solution (80 wt % in water), and 313.6 μL of ammonia solution (25 wt % in water) in a 100 mL flask. After being vigorously stirred for 10 min, the mixture was refluxed at 95 °C for 2 h and cooled to room temperature, forming a black graphene aqueous dispersion. Graphene paper was prepared by filtration of the graphene dispersion, similar to the method for making GO paper. (For depositing PANI on GO or graphene paper, the Millipore filter was retained during the polymerization process and peeled off after the final drying.)

2.2.4. ***Preparation of GO−PANI and Graphene−PANI Hybrid Papers.*** A typical rapid-mixture polymerization was performed in a 100 mL glass beaker. Aniline (6.4 mmol) was dissolved in 20 mL of 1 M HCl solution and APS (1.6 mmol) was dissolved in 20 mL of the same HCl solution. The two solutions were rapidly poured together and immediately stirred to ensure sufficient mixing before the polymerization began. After being stirred strongly for 30s, the solution was stopped stirring and the GO or graphene paper containing filter was carefully immersed into it. Reactions were carried out at room temperature for 24 h without stirring, and the papers were then collected, washed with water 5 times, dried at room temperature in air, and peeled off from the filter. Meantime, the aqueous phases were also collected and purified by centrifugation against water. When the water bath reached a pH value of 6, the dark green powder products were collected and dried in a vacuum at 60 °C.

2.3. Characterization of Structure and Properties. Field-emission scanning electron microscope (FESEM, JSM 6701F) was employed to investigate the morphology of the samples. The XPS measurements of the graphite powders, GO and graphene papers were performed on a Perkin-Elmer PHI-5702 multifunctional X-ray photoelectron spectroscope (Physical Electronics, USA), using Al−Kα radiation (photon energy 1476.6 eV) as the excitation source and the binding energy of Au (Au $4f_{7/2}$: 84.00 eV) as the reference. Fourier transformation infrared (FTIR) spectra were recorded using a Bruker IFS66 V FTIR spectrometer, Raman spectra were recorded using a micro-Raman spectroscopy (JY-HR800, the excitation wavelength at 532 nm), and X-ray diffraction (XRD) patterns were carried out by a X-ray diffraction using Cu *K*α radiation (XRD, Philips X'Pert Pro.), to investigate the structures and compositions of the samples.

The electrochemical properties of the paperlike samples were carried out using CHI660C Electrochemical Working Station (ChenHua, China) in a conventional Teflon electrochemistry cell with a three-electrode system in 1 M H_2SO_4 electrolyte at room temperature: a working electrode (WE), a platinum wire counter electrode and an Ag/AgCl (sat. KCl) reference electrode. Each paper-like sample was directly used as a working electrode and the exposed area of the working electrode to the electrolyte is about 0.28 cm^2. Because the diameter of all the papers is 39 mm, the mass of the exposed electrodes could be calculated out after measuring the masses of the whole papers, which are all on the order of $\sim 1 \times 10^{-4}$ g (0.30 mg for GO paper, 0.35 mg for GO−PANI paper, 0.21 mg for graphene paper, and 0.22 mg for graphene−PANI paper). The cyclic voltammetry (CV) curves were collected with a potential window from −0.2 to 1.0 V versus SCE at a scan rate of 10 mV/s. Electrochemical impedance spectroscopy (EIS) measurements were recorded from 10 kHz to 10 mHz with an alternate current amplitude of 5 mV. Galvanostatic charge/discharge measurements were run on from 0 to 0.8 V at a current density of 400 mA/g, and open circuit potential. The *C* was calculated from the slope of the discharge curve, according to the equation $C = (I\Delta t)/(\Delta V m)$, where *C* is the specific capacitance, *I* is the constant discharge current, Δt is the discharge time, ΔV is the voltage difference in discharge, and *m* is the mass of the exposed working electrode.

2.4. Biocompatibility Test. 2.4.1. ***Cell Culture.*** L-929 cells were routinely cultured in DMEM containing 10% FBS and incubated at 37 °C in a humidified chamber with 10% CO_2. The culture medium was refreshed every 2 days. When the cells

became almost confluent, they were released by treating with 0.25% trypsin-EDTA solution for 3 min at 37 °C and resuspended in the DMEM with a final concentration of 1×10^4 cells/mL.

2.4.2. *In vitro Cytocompatibility Assay.* Before the biocompatibility tests, all of the paperlike samples were cut by scissors into quadrate pieces of approximately 5 mm × 5 mm, thermally annealed at 100 °C under vacuum, and pasted on silicon substrates with the same sizes. In vitro cytocompatibility was investigated by MTT colorimetric assay. Briefly, each sample was placed into a 24-well culture plate and exposed to UV light for 30 min to sterilize, and then was equilibrated with prewarmed DMEM medium at 37 °C for 2 h. After the wells were removed from the medium, quantitative cells (30 000 cells/well) were seeded onto each sample surface, allowing them to incubate for 48 and 96 h, respectively. At the prescribed time point, 100 μL of MTT phosphate buffer solution (PBS) (5 mg/mL) was added into each well containing the test sample and culture medium. The culture plate was then kept at 37 °C for 4 h. At the end of the incubation, the supernatant was removed and 1 mL of DMSO was added into each well. The culture plate was shaken to dissolve the purple formazan crystals and the optical density (OD) value of the resulting solution was recorded using a microplate reader (Model 550, BIO-RAD, Japan) at the wavelength of 490 nm. The assay was conducted in triplicate for each sample and three parallel experiments were performed. Data were expressed as the mean ± SD (standard deviation) from the three independent experiments. Statistical analysis was performed with Student's t test and values were considered to be significantly different when $p < 0.05$. To calibrate the cellular survival rate, we set blank and control groups. In the blank group, only culture media was added into the well. In the control group, cells and culture media without samples were added. The blank and control groups were treated with the same procedures and incubated for the same time as those in the experimental group. The measured OD values of the blank, control, and experimental groups were coded as OD_{bla}, OD_{con}, and $OD_{exp,}$ respectively. Finally, the cellular survival rate was calculated by the following equation: survival rate $= OD_{exp} - OD_{bla}/OD_{con} - OD_{bla}$.

2.4.3. *Acridine Orange Staining for Fluorescence Investigation.* After being seeded for 48 and 96 h, the graphene−PANI samples were rinsed in PBS (pH 7.4), and the cells were then fixed in the ethanol for 10 min. Subsequently, the cells attached to the samples' surfaces were stained with acridine orange fluorescent dye in PBS solution (pH 7.4) for 3 min and examined by a fluorescence microscope (BX51, Olympus, Japan).

2.4.4. *Preparation of Sample for SEM Investigation.* Briefly, after being cultured for 48 h, the cells attached on the graphene-PANI sample was washed with PBS (pH = 7.4), fixed by 2.5 wt % glutaraldehyde in PBS at 4 °C for 2 h, rinsed with PBS, fixed again by 1 wt % osmium tetroxide in PBS at 4 °C for 1 h. Finally, standard dehydration in an ethanol graded series (50, 70, 95, and 100%) and critical point drying were performed. Finally, the sample was coated with gold in a vacuum for the investigation of SEM.

RESULTS AND DISCUSSION

The X-ray photoelectron spectroscopy (XPS) spectra of the parent graphite powders, GO and graphene papers (see Figure S1 in the Supporting Information) indicate the considerable degree of the oxidation for GO and the subsequent reduction for graphene. Compared with graphite, the C1s XPS spectrum of GO indicates the presence of four components: the C in C═C bonds (284.5 eV), the C in C−O bonds (286.6 eV), the C in C═O bonds (287.7 eV), and the C in O−C═O bonds (288.7 eV) (8, 11). Compared with GO, although the C1s XPS spectrum of graphene also presents the same components, the intensity of the peak attributed to C−C bonds is dominant in the spectrum and the peaks corresponded to the oxygen functionalized C are much smaller than those in GO, suggesting considerable deoxygenation by reduction process. Moreover, an additional component corresponding to C in C−N bonds (285.8 eV) appears that indicates the incorporation of nitrogen come from hydrazine.

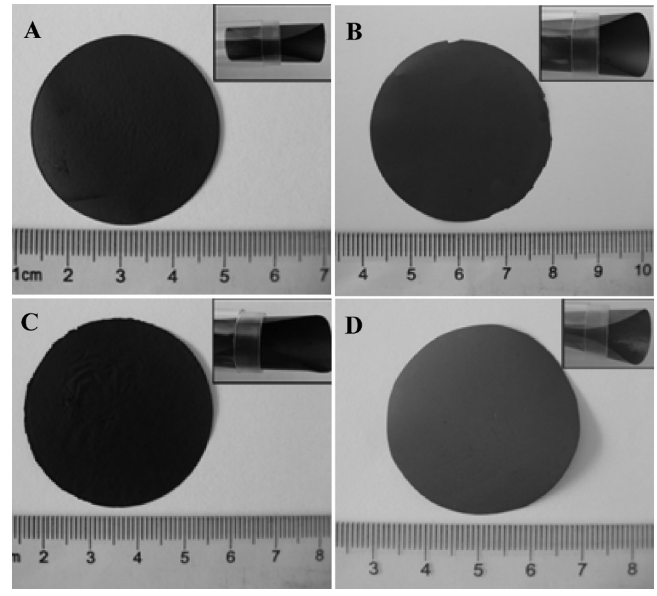

FIGURE 1. Digital camera images (A) of free-standing GO paper, (B) graphene paper, (C) GO−-PANI paper, and (D) graphene−PANI paper. The inset images indicate the flexibility of the samples.

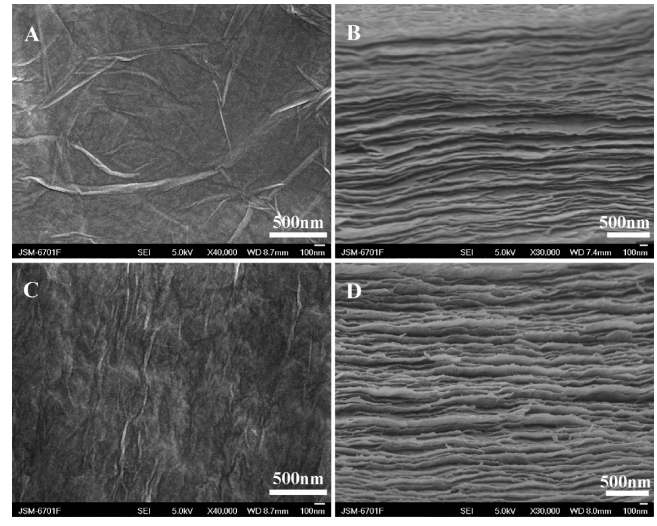

FIGURE 2. SEM images of (A, B) GO paper and (C, D) graphene paper. A and C are top-view images and C and D are side-view images.

We observe that as-prepared free-standing GO and graphene papers both are flexible and black, and graphene paper displays a weak metallic luster on the surface (Figures 1A and 2B). High-resolution SEM analyses reveal that the surfaces of the GO and graphene papers both are quite smooth except a few of folds (Figure 2A,C). The fracture edges of the papers reveal well-compact layer-by-layer stacking through almost the entire cross-section and the

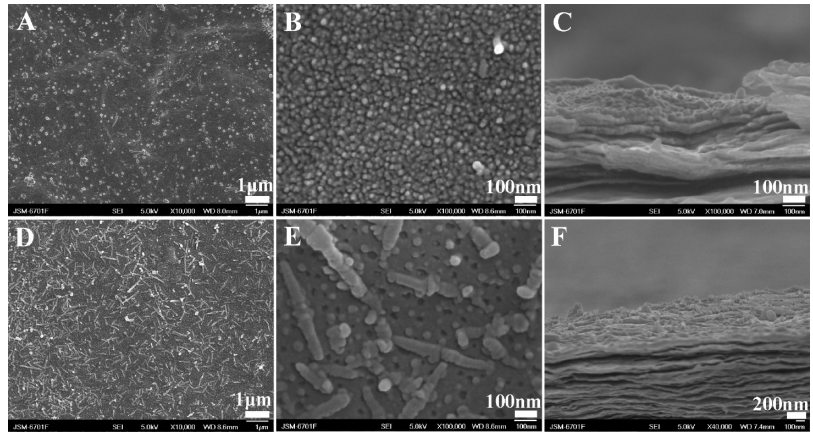

FIGURE 3. Top-view SEM images of (A, B) GO−PANI paper and (D, E) graphene−PANI paper. Side-view SEM images of (C) GO−PANI paper and (F) graphene−PANI paper.

distance between less densely packed 'wavy' skin layers is about 100−200 nm thick (Figure 2B,D), which is the same as the microstructures of the GO and graphene papers obtained by Ruoff and Li, respectively (13, 15). In addition, the GO and graphene papers have the similar thickness of 4−5 μm (see Figure S2 in the Supporting Information).

We find that after rapid-mixture polymerization of aniline monomers in the presence of GO or graphene papers, the entire water phase is filled homogeneously with dark-green PANI. Interestingly, after collecting, washing and drying papers, the surface color of GO paper is changed to dark purple, whereas the surface color of graphene paper is changed to dark gold. It indicates that there is obvious difference in the microstructure or morphology between PANI deposited on GO paper and that deposited on graphene paper. The difference is evident from their SEM images. As seen from images A and B in Figure 3, the dark-purple coating is consisted of dominant small-compact nanoparticles and some scattered large nanoparticles. The diameter of the compact PANI nanoparticles is about 15−30 nm. Likewise, as seen from images D and E in Figure 3, the dark-gold coating is consisted of a continuous film containing a large quantity of nanorods and nanoparticles. The nanorods are adsorbed on the surface with the diameter of tens of nanometers and the length of hundreds of nanometers. In addition, there are some nanopores existing on the surface of the film.

Cross-section SEM images (Figure 3C,F) exhibit the PANI films on the surfaces of the two hybrid papers are quite thin and the thicknesses is both just tens of nanometers. For GO−PANI paper, the thickness of PANI coating is very similar to the diameter of the compact nanoparticles, suggesting the coating is monolayer consisted of nanoparticles. It is known that high quality PANI nanofibers can be prepared using rapid-mixture polymerization (28). In this process, because the monomer aniline and the initiator APS are mixed completely before the reaction, almost all the reactants are quickly consumed during the initial polymerization so that secondary growth of the newly generated PANI can be suppressed effectively (28). In our synthesis process, we believe that after immersing the GO (or graphene) paper into the mixture of aniline and APS solutions, aniline monomers adsorbed and adjacent to the surface will react to generate PANI nanoparticles (or ultrathin film, which will be deposited on the surface of the paper in the early stage of polymerization. Because no reactants will be available for further reaction, the diameter of the PANI nanoparticles (or thickness of the film) can not be increased remarkably during further slow polymerization reaction for 24 h. This effect explains why PANI coatings are very thin for GO−PANI and graphene−PANI hybrid papers. It is well-known that the carboxylic and phenolic hydroxyl groups exist on the GO sheets (29, 30). In our experiments, we believe that as soon as the GO paper is immersed into aqueous phase, the aniline monomers will be preferentially adsorbed on the sites containing carboxylic and phenolic hydroxyl groups by hydrogen bonds or with van der Waals attractions. Thus, these sites will act as the "seeding dots" to form PANI nanoparticles. On the contrary, it is also known that the oxygen functionalized groups on the planar surfaces of GO sheets will be reduced by hydrazine and the as-prepared graphene sheets are electro-neutral in acidic aqueous phas e (15). Thus, we believe that adsorption probability of aniline monomers on the whole surface of graphene paper is equipotent, resulting in the formation of continuous PANI film. In our synthesis process, the dark-green PANI in aqueous phase is also collected by centrifugation. SEM image (see Figure S3 in the Supporting Information) reveals the dark-green powders are almost PANI nanofibers with the diameter of tens of nanometers and a few of nanoparticles. Thus, we suppose that the scattered large particles (shown in Figure 3A) are derived from the adsorption of the PANI nanoparticles generated in the aqueous phase, during the further slow polymerization. Also, the nanorods and nanoparticles (shown in Figure 3D and 3E) are come from the adsorption of short PANI nanofibers and PANI nanoparticles generated in the aqueous phase. Moreover, we guess that the generation of nanoscale pores on the surface of the PANI film (shown in Figure 3E) might be due to that some weakly adsorbed PANI nanoparticles would be removed during the subsequent washing procedure. It should be mentioned that the reason why the short PANI nanofibers are adsorbed on the surface of graphene−-PANI paper instead of GO−PANI paper is still not clear. In addition, whether for GO−PANI or

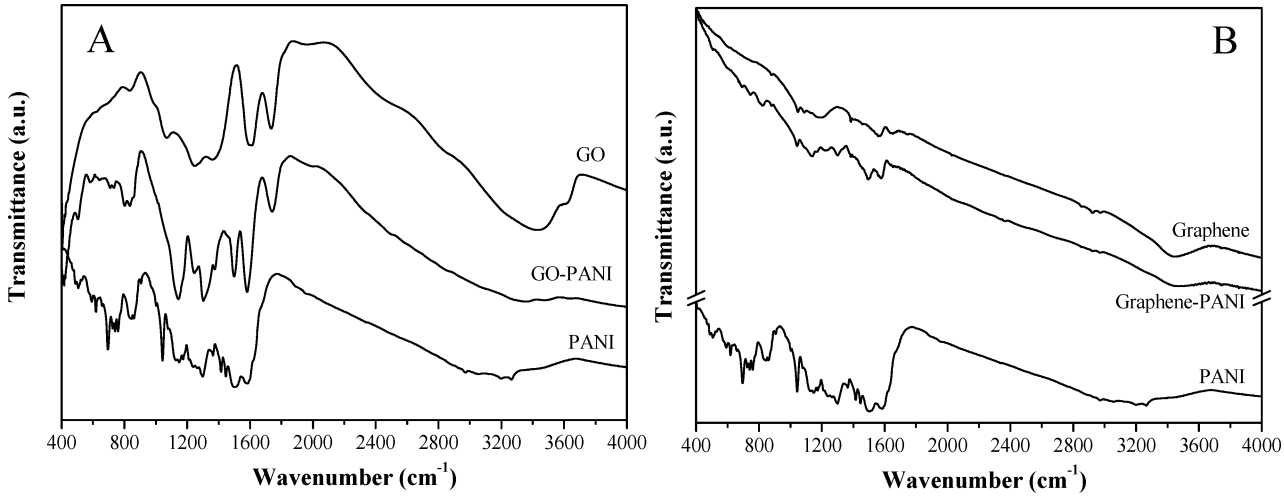

FIGURE 4. (A) FTIR spectra of GO paper, GO−PANI paper, and PANI powder samples. (B) FTIR spectra of graphene paper, graphene−PANI paper, and PANI powder samples.

graphene−PANI hybrid paper, the PANI is just deposited on the outermost layer instead of every layer through the entire cross-section. It is mainly due to the GO or graphene paper being thick and stacked so that the reactants and the newly generated PANI cannot enter the inside of the paper. Similar to GO and graphene papers, the as-prepared hybrid papers can be rolled up or bent easily, suggesting good flexibility (Figure 1C,D). Consequently, the deposition of PANI coatings on GO and graphene papers using rapid-mixture polymerization exhibits great advantages over the traditional chemical polymerization and electro-polymerization: (1) The process is quite simple and large area deposition can be realized without the need of the costly apparatus and any the assistance of heating or cooling. (2) Secondary growth of PANI is limited, resulting in ultrathin PANI coatings with high specific surface area, which are unlikely to destroy the flexibility of the pristine GO and graphene papers.

To verify the composition of PANI, we measured the infrared spectra of the products. As shown in Figure 4a, for the PANI powder sample, the broad peak in the frequency range of 3200−3500 cm^{-1} is attributable to the N−H stretching vibrations of the emeraldine salt. The weak shoulders at 2980−3050 cm^{-1} correspond to aromatic sp^2 CH stretching (31). The absorption peaks located at 1570 and 1492 cm^{-1} are respectively ascribed to the C═C stretching deformation of the quinoid ring and benzenoid rings in the emeraldine salt (32). The peaks at 1302 and 1152 cm^{-1} correspond to C−N stretching of the secondary aromatic amine and C═N stretching, respectively (33). The peaks at 1130 and 835 cm^{-1} are attributed to the aromatic C−H bending in the plane and out of the plane for the 1, 4-disubstituted aromatic ring (31). For the GO paper, the characteristic vibrations include the broad and intense O−H peak at 3400 cm^{-1}, strong C═O peak in carboxylic acid and carbonyl moieties at 1732 cm^{-1}, C−OH peak at 1365 cm^{-1}, C−O−C peak at 1246 cm^{-1}, C−O stretching peak at 1065 cm^{-1}, and aromatic C−H peak at 832 cm^{-1} (34). The peak centered at 1590−1620 cm^{-1} is assigned to adsorbed water molecules, but may be also containing components from skeletal vibrations of unoxidized graphitic domains (8, 35). By comparison, the spectrum of the GO−PANI hybrid paper illustrates the obvious presence of PANI characteristic vibrations, suggesting PANI can be successfully deposited on the GO surface. For the graphene paper (Figure 4B), the obvious broad peak at 3200−3600 cm^{-1} is attributed to N−H bonds, the peaks between 1100 and 1650 cm^{-1} are associated with the stretching vibrations of both double and single C−N and C−C bonds, and the stretching of C−H bonds. Because the overlapping of the strong adsorption of graphene sheets in this region, the precise classification is not feasible as that did for GO. Of course, by comparison, it is still clear that the spectrum of the graphene−PANI hybrid paper presents the C═C stretching deformation of the benzenoid rings at 1492 cm^{-1}, suggesting PANI can also be successfully deposited on the graphene surface.

Raman spectroscopy provides a powerful tool to determine the microstructure of carbon-based materials and PANI polymer. Therefore, we performed Raman measurements on the paperlike GO, graphene, GO−PANI, and graphene−PANI samples and PANI powder sample. As shown in Figure 5A, the Raman spectrum of GO displays two prominent peaks at 1371 and 1627 cm^{-1}, corresponding to the well-documented D and G bands, respectively. Although the Raman spectrum of graphene also has both D and G bands at 1365 and 1617 cm^{-1}, respectively, the intensity ratio of D/G is increased obviously in comparison with that of the GO spectrum. It agrees well with that reported by Stankovich (12), indicating the realization of deoxygenation in chemically reduced graphene. For the Raman spectrum of GO−PANI sample, apart from the D and G bands of GO, three new representative peaks arising from PANI can be indexed at 1513, 1180, and 814 cm^{-1}, which correspond to C═C stretching vibration of quinoid ring, C−H bending of the quinoid ring and substituted benzene ring deformation, respectively (33, 36). Similarly, for the Raman spectrum of graphene-PANI sample, the new peaks arising from PANI at 1180 and 814 cm^{-1} also appeal, apart from the D and G bands of graphene paper. This presence of these new peaks indicates the generation of PANI on the surfaces of the GO and graphene papers.

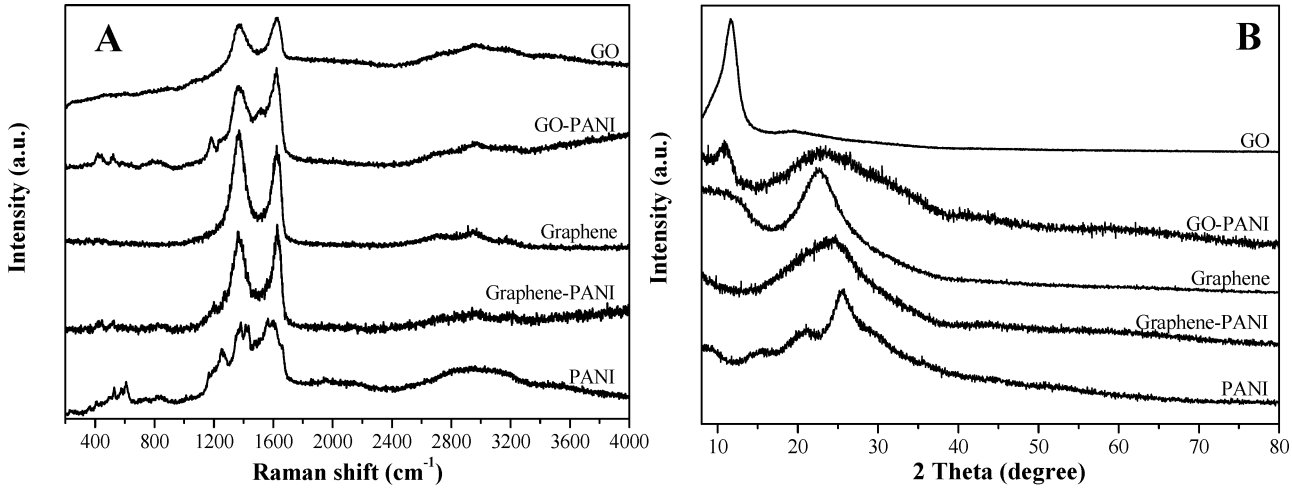

FIGURE 5. (A) Raman spectra and (B) XRD patterns of GO paper, GO−PANI paper, graphene paper, graphene−PANI paper, and PANI powder samples.

To further evaluate the quality of the hybrid papers, we employed XRD measurements. As shown in Figure 5B, the XRD pattern of whether the GO paper or the graphene paper exhibits only one peak, centered at 11.6 and 22.6°, respectively. For comparison, there is a new broad peak at 15−35° existing in the XRD pattern of the GO−PANI paper, which is ascribed to the reflection of PANI. Although the XRD pattern of the graphene−PANI paper just exhibits one peak similar to that of GO paper, the center position shifts up obviously and the peak has widened in comparison with that of the GO pattern, apparently as a result of the influence come from PANI. Therefore, the XRD result further confirms the formation of PANI coatings on the surfaces of the GO and graphene papers, which is consistent with that of FTIR and Raman investigations.

The electrochemical performances of the paper-like samples were analyzed using cyclic voltammetry (CV), electrochemical impedance spectroscopy (EIS), and galvanostatic charge/discharge. The capacitance estimated from the CV curve was reported by integrating over the full CV curve to determine the average value (37). From the CV curves shown in Figure 6A, the remarkable difference of electrochemical surface activity among GO, GO−PANI, graphene, and graphene−PANI papers can be easily recognized. In detail, the GO electrode exhibits very low current density response (the peak current density is on the order of $\sim 1 \times 10^{-3}$ A/g, shown as the inset in Figure 6A). The existence of redox peaks is due to the large number of oxygen-containing functional groups on GO surfaces, which are likely to play a key role in electrochemical activity of GO. This phenomenon directly reflects the electrically insulating of GO and hence the use of GO paper such as an electrode material is not possible. However, compared with the GO electrode, the current density response and the CV curve area of the GO−PANI electrode are both much larger than those of the GO electrode. This indicates that the electrochemical performances of the GO-PANI hybrid papers are remarkably enhanced owing to the addition of PANI coating on the surface of the GO paper. Similarly, the graphene electrode presents one pair of weak redox peaks due to the transition between quinone/hydroquinone groups, which is typical for carbon materials (26, 38). However, compared with the graphene electrode, two couples of redox peaks (0.33 V/0.15 V, 0.59 V/0.36 V) appear in the CV curve of the graphene−PANI electrode, which are attributed to the transitions between a semiconducting state (leucoemeraldine form) and a conducting state (polaronic emeraldine form) and the Faradaic transformation of emeraldine−pernigraniline, respectively (26).

The EIS data were analyzed using Nyquist plots, which show the frequency response of the electrode/electrolyte system and are the plots of the imaginary component (Z″) of the impedance against the real component (Z′). From the Nyquist plots shown in Figure 6B, all the plots of the GO−PANI, graphene, and graphene−PANI electrodes display a small semicircle at high frequency followed by a transition to linearity at low frequency. Also, these plots have a slope portion close to 45° at low frequency. This is typical of Warburg impedance and is a result of the frequency dependence of ion diffusion/transport in the electrolyte (37). As seen from Figure 6B, the Warburg curves are unnoticeable for the graphene and graphene−PANI electrodes, indicating the two electrodes have short ion diffusion path. This shall facilitate the efficient access of electrolyte ions to the surfaces of the graphene and graphene−PANI electrodes (39). Impedance measurements can provide useful information about the equivalent series resistance (ESR) and the maximum power density (P_{max}) of a supercapacitor. The intersection of the plots at the *X*-axis represents the ESR of the electrode which determines the charge/discharge rate of the electrode (37). As seen form Figure 6B, it is apparent that the ESR of the GO−PANI, graphene, and graphene−PANI electrodes is 40.2, 39.9, and 21.4 Ω, respectively. Also, ESR is an importance factor in determining the power density of a supercapacitor (37). According to the equation $P_{max} = V_i^2/4mR$, where V_i is the initial voltage, R is the ESR, and m is the mass of the exposed electrode, the P_{max} of the GO−PANI, graphene, and graphene−PANI electrodes can be calculated as 11.4, 19.1, and 33.9 kW/kg, respectively. The P_{max} of the paperlike electrodes is larger than that of the

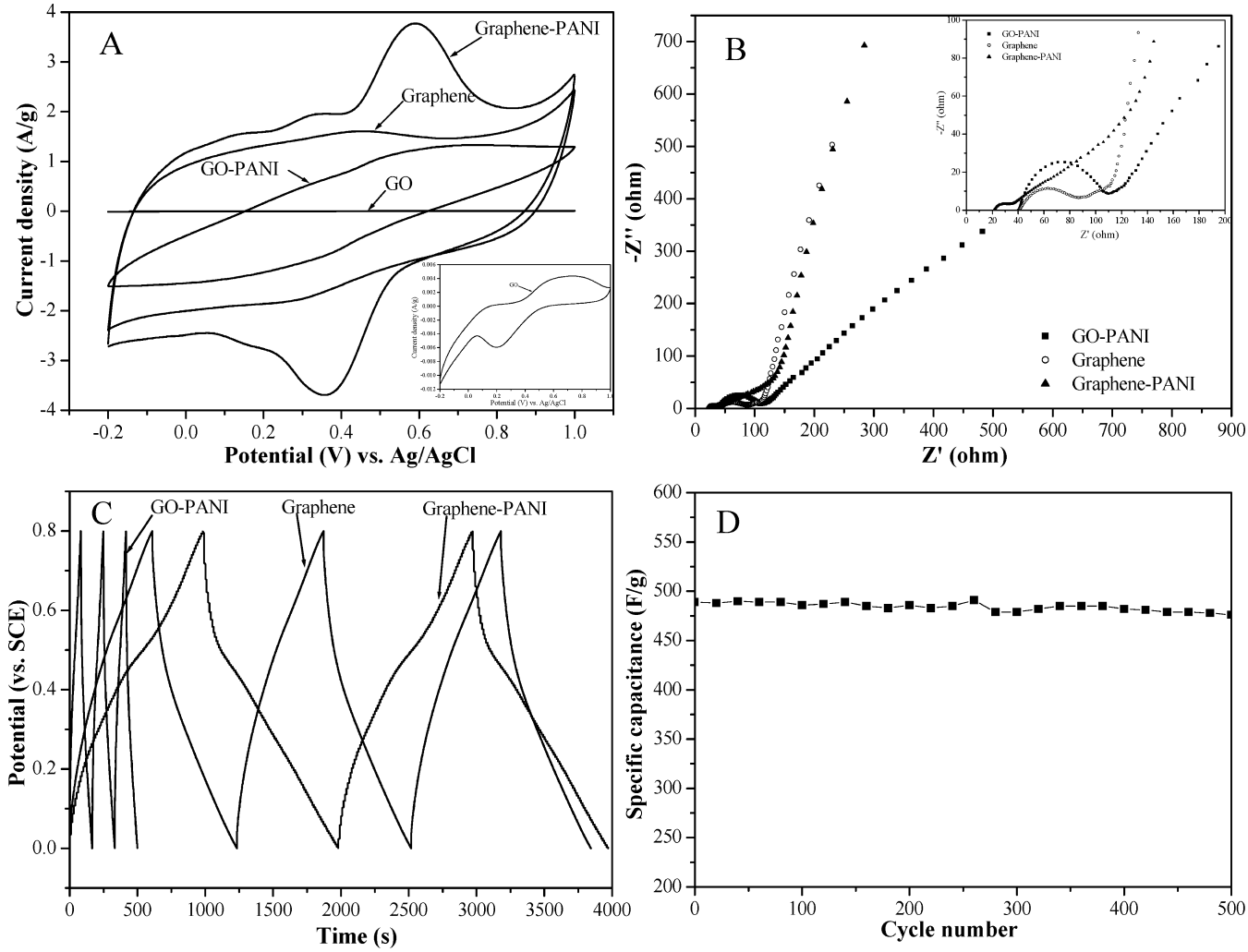

FIGURE 6. (A) CV of GO, GO−PANI, graphene, and graphene−PANI paperlike electrodes in 1 M H_2SO_4 solution at 10 mV s^{-1}. (B) Nyquist plots of GO−PANI, graphene, and graphene−PANI paperlike electrodes. Inset is the enlarged plots of the high-frequency region. (C) Galvanostatic charge−discharge curves of GO−PANI, graphene, and graphene−PANI paperlike electrodes at 400 mA/g. (D) Variation of the specific capacitance of graphene−PANI paperlike electrode with cycle number at 400 mA g^{-1}.

graphene materials (10 kW/kg) reported by Chen et al. (39). The high value of the power density for our electrodes shall be well-suited for surge-power delivery application (40).

Galvanostatic charge−discharge properties of the paperlike samples were performed at a constant current density of 400 mA/g. According to the capacitance equation evaluated from the slopes of the discharge curves (shown in the Experimental Section), the specific capacitance of GO−PANI, graphene, and graphene−PANI electrodes can reach 42, 366, and 489 F/g at 400 mA/g, respectively. It indicates that the specific capacitance of the hybrid papers is remarkably enhanced compared with the corresponding parent GO and graphene papers. Meng et al. reported that the specific capacitance of pure PANI nanofibers is about 275 F/g at 200 mA/g (41). Therefore, we believe that the high specific capacitance in our graphene−PANI system is probably due to the combination effect of the compact layer-by-layer structure of graphene paper, the high specific surface area of PANI nanostructures, and the synergistic interaction between PANI and graphene sheets. In addition, as shown in Figure 6D, the specific capacitance of the graphene−PANI electrode in our system still remains above 475 $F \cdot g^{-1}$ at 400 mA/g after 500 cycles (above 96% of the original value), illustrating this electrode possesses good cycling stability and lifetime. Therefore, these paperlike products, especially the graphene−PANI hybrid paper, have great potential applications in flexible supercapacitors.

In this paper, to study the biocompatibility of the paperlike samples, the mouse fibroblast cell line L929 was used, which is commonly used to assess cytotoxicity of potential substrates for cell growth, and has been used previously in biocompatibility testing of carbon nanotubes network (42). To evaluate the in vitro cytocompatibility of the samples, we performed MTT colorimetric assay. As shown in Figure 7, after 48 h of cell seeding, the cell survival rate on the GO−PANI hybrid paper is about 6% higher than that on the GO paper and the survival rate on the graphene−PANI hybrid paper is about 9% higher than that on the graphene paper. After 96 h of cell seeding, the survival rate on the GO−PANI is about 5% higher than that on the GO paper and the survival rate on the graphene−PANI is about 8% higher than that on the graphene paper. This indicates that the PANI coatings on GO and graphene papers can enhance the cell proliferation of the corresponding parent papers. It can be

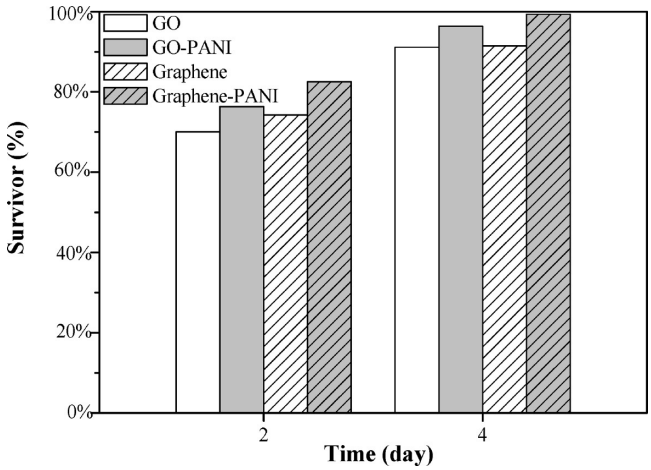

FIGURE 7. Survivor ratio of LG9-9 cells on GO, GO–PANI, graphene, and graphene–PANI papers after 2 and 4 days, respectively.

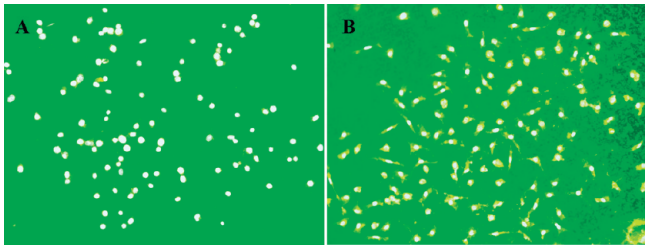

FIGURE 8. Fluorescence microscopy images of L-929 cells growing on graphene-PANI paper for (A) 2 and (B) 4 days. The magnification is 100×.

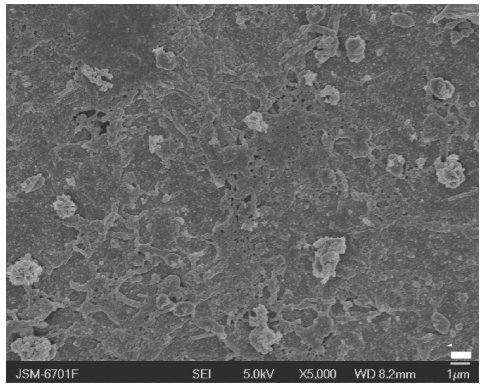

FIGURE 9. SEM image of L-929 cells growing on graphene–PANI paper for 2 days.

definitely attributed to the excellent intrinsic biocompatibility and the hydrophilic nature of PANI materials, which can greatly promote the cell-material interaction (43). Moreover, it is noteworthy that the graphene–PANI hybrid paper exhibits best biocompatibility among these paperlike samples. In addition, the cell growth onto the graphene–PANI hybrid paper and the cell morphology were determined using fluorescence microscopy and SEM, respectively. The fluorescent staining shown in Figure 8 reveals that L-929 cells are well adhered and proliferated on the graphene–PANI hybrid paper with the increase of the culture time. The SEM image shown in Figure 9 presents the specific morphology of L-929 cells on the graphene-PANI hybrid paper. After 2 days of growth, fibroblasts have formed a confluent layer covering the surface of the paper, i.e., most of the surface of the paper is hidden beneath the cell layer. Therefore, on the basis of the above investigations, the graphene–PANI hybrid paper can offer an ideal biocompatible platform for cell culture.

CONCLUSIONS

In summary, we have demonstrated that free-standing GO–PANI and graphene–PANI hybrid papers can be prepared by simple rapid-mixture polymerization using GO and graphene papers as substrates, respectively. The obtained hybrid papers maintain the pristine flexibility of GO and graphene papers, and display improved electrochemical performances and biocompatibility. The remarkable combination of advantages coming from graphene (and GO) papers and nanostructural PANI, including flexibility, electrochemical activity and capacitance, and biocompatibility, making such paperlike hybrid papers promising materials for various applications in biosciences, such as flexible bioelectrodes and batteries, biosensors, bioengineering, and culture of electrically excitable cells.

Acknowledgment. The authors acknowledge the support from the Top Hundred Talents Program of Chinese Academy of Sciences. The authors thank Mr. Sheng Liu for electrochemical measurements and Mr. Dong Zhang for biocompatibility assessment. The authors gratefully acknowledge the School of Stomatology, Lanzhou University, for access to the cell culture and MTT colorimetric assay.

Supporting Information Available: C1s XPS spectra of graphite powders, GO, and graphene papers; side-view SEM image of graphene paper; and SEM image of PANI powders (PDF). This material is available free of charge via the Internet at http://pubs.acs.org.

REFERENCES AND NOTES

(1) Kim, K. S.; Zhao, Y.; Jang, H.; Lee, S. Y.; Kim, J. M.; Kim, K. S.; Ahn, J. H.; Kim, P.; Choi, J. Y.; Hong, B. H. *Nature* **2009**, *457*, 706.
(2) Geim, A. K.; Novoselov, K. S. *Nat. Mat.* **2007**, *6*, 183.
(3) Kopelevich, Y.; Esquinazi, P. *Adv. Mater.* **2007**, *19*, 4559.
(4) Lee, D. H.; Kim, J. E.; Han, T. H.; Hwang, J. W.; Jeon, S.; Choi, S. Y.; Hong, S. H.; Lee, W. J.; Ruoff, R. S.; Kim, S. O. *Adv. Mater.* **2010**, *22*, 1247.
(5) Han, T. H.; Lee, W. J.; Lee, D. H.; Kim, J. E.; Choi, E. Y.; Kim, S. O. *Adv. Mater.* **2010**, *22*, 2060.
(6) Novoselov, K. S.; Geim, A. K.; Morozov, S. V.; Jiang, D.; Zhang, Y.; Dubonos, S. V.; Grigorieva, I. V.; Firsov, A. A. *Science* **2004**, *306*, 666.
(7) Berger, C.; Song, Z. M.; Li, X. B.; Wu, X. S.; Brown, N.; Naud, C.; Mayou, D.; Li, T. B.; Has, J.; Marchenkov, A. N.; Conrad, E. H.; First, P. N.; Heer, W. A. *Science* **2006**, *312*, 191.
(8) Xu, Y.; Bai, H.; Lu, G.; Li, C.; Shi, G. *J. Am. Chem. Soc.* **2008**, *130*, 5856.
(9) Tung, V. C.; Allen, M. J.; Yang, Y.; Kaner, R. B. *Nat. Nanotechnol.* **2008**, *4*, 25.
(10) Stankovich, S.; Piner, R. D.; Chen, X. Q.; Wu, N. Q.; Nguyen, S. T.; Ruoff, R. S. *J. Mater. Chem.* **2006**, *16*, 155.
(11) Stankovich, S.; Dikin, D. A.; Dommett, G. H. B.; Kohlhaas, K. M.; Zimney, E. J.; Stach, E. A.; Piner, R. D.; Nguyen, S. T.; Ruoff, R. S. *Nature* **2006**, *442*, 282.
(12) Stankovich, S.; Dikin, D. A.; Piner, R. D.; Kohlhaas, K. A.; Kleinhammes, A.; Jia, Y. Y.; Wu, Y.; Nguyen, S. T.; Ruoff, R. S. *Carbon* **2007**, *45*, 1558.
(13) Dikin, D. A.; Stankovich, S.; Zimney, E. J.; Piner, R. D.; Dommett, G. H. B.; Evmenenko, G.; Nguyen, S. T.; Ruoff, R. S. *Nature* **2007**, *448*, 457.
(14) Chen, C. M.; Yang, Q. H.; Yang, Y. G.; Lv, W.; Wen, Y. F.; Hou, P. X.; Wang, M. Z.; Cheng, H. M. *Adv. Mater.* **2009**, *21*, 1.

(15) Li, D.; Müller, M. B.; Gilje, S.; Kaner, R. B.; Wallace, G. G. *Nat. Nanotech.* **2008**, *3*, 101.
(16) Chen, H. Q.; Müller, M. B.; Gilmore, K. J.; Wallace, G. G.; Li, D. *Adv. Mater.* **2008**, *20*, 3557.
(17) Pitkethly, M. J. *Nano Today* **2004**, *7*, 20.
(18) MacDiarmid, A. G. *Angew. Chem., Int. Ed.* **2001**, *40*, 2581.
(19) Gu, Z. M.; Zhang, L.; Li, C. Z. *J. Macromol. Sci., Part B: Phys.* **2009**, *48*, 226.
(20) Seredych, M.; Pietrzak, R.; Bandosz, T. J. *Ind. Eng. Chem. Res.* **2007**, *46*, 6925.
(21) Bissessur, R.; Liu, P. K. Y.; White, W.; Scully, S. F. *Langmuir* **2006**, *22*, 1729.
(22) Wang, G. C.; Yang, Z. Y.; Li, X. W.; Li, C. Z. *Carbon* **2005**, *43*, 2564.
(23) Murugan, A. V.; Muraliganth, T.; Manthiram, A. *Chem. Mater.* **2009**, *21*, 5004.
(24) Wang, H. L.; Hao, Q. L.; Yang, X. J.; Lu, L. D.; Wang, X. *Electrochem. Commun.* **2009**, *11*, 1158.
(25) Wang, D. W.; Li, F.; Zhao, J. P.; Ren, W. C.; Chen, Z. G.; Tan, J.; Wu, Z. S.; Gentle, L.; Lu, G. Q.; Cheng, H. M. *ACS Nano* **2009**, *3*, 1745.
(26) Zhang, F.; Kang, E. T.; Neoh, K. G.; Wang, P.; Tan, K. L. *Biomaterials* **2002**, *23*, 787.
(27) Hummers, W. S.; Offerman, R. E. *J. Am. Chem. Soc.* **1958**, *80*, 1339.
(28) Huang, J.; Kaner, R. B. *Angew. Chem., Int. Ed.* **2004**, *43*, 5817.
(29) Lerf, A.; He, H. Y.; Forster, M.; Klinowski, J. *J. Phys. Chem. B* **1998**, *102*, 4477.
(30) Szabó, T.; OttóPéter-Forgó, B.; Katalin, J.; Yiannis, S.; Dimitris, P.; Imre, D. *Chem. Mater.* **2006**, *18*, 2740.
(31) Yan, X. B.; Han, Z. J.; Yang, Y.; Tay, B. K. *Sens. Actuators B* **2007**, *123*, 107.
(32) Cruz-Silva, R.; Romero-Garcia, J.; Angulo-Sanchez, J. L.; Flores-Loyola, E.; Farias, M. H.; Castillon, F. F.; Diaz, J. A. *Polymer* **2004**, *45*, 4711.
(33) Tiwaria, A.; Kumar, R.; Prabaharan, M.; Pandey, R. R.; Kumari, P.; Chaturvedi, A.; Mishra, A. K. *Polym. Adv. Technol.* **2009**; DOI: 10.1002/pat.1470.
(34) Si, Y. C.; Samulski, E. T. *Nano Lett.* **2008**, *8*, 1679.
(35) Stankovich, S.; Piner, R. D.; Nguyen, S. T.; Ruoff, R. S. *Carbon* **2006**, *44*, 3342.
(36) Li, X.; Gao, Y.; Gong, J.; Zhang, L.; Qu, L. *J. Phys. Chem. C* **2009**, *113*, 69.
(37) Stoller, M. D.; Park, S.; Zhu, Y. W.; An, J. H.; Ruoff, R. S. *Nano Lett.* **2008**, *8*, 3498.
(38) Nian, Y. R.; Teng, H. S. *J. Electrochem. Soc.* **2002**, *149*, A1008.
(39) Wang, Y.; Shi, Z. Q.; Huang, Y.; Ma, Y. F.; Wang, C. Y.; Chen, M. M.; Chen, Y. S. *J. Phys. Chem. C* **2009**, *113*, 13103.
(40) Du, C. S.; Yeh, J.; Pan, N. *Nanotechnology* **2005**, *16*, 350.
(41) Meng, C. Z.; Liu, C. H.; Fan, S. S. *Electrochem. Commun.* **2009**, *11*, 186.
(42) Correa-Duarte, M. A.; Wagner, N.; Rojas-Chapana, J.; Morsczeck, C.; Thie, M.; Giersig, M. *Nano Lett.* **2004**, *4*, 2233.
(43) Crawford, G. A.; Chawla, N.; Das, K.; Bose, S.; Bandyopadhyay, A. *Acta Biomaterial* **2007**, *3*, 359.

AM100293R